ROYAL SOCIETY
OF CHEMISTRY

PAPER

Check for updates

Unveiling structural and energetic characterization of the emissive RNA alphabet anchored in the methylthieno[3,4-*d*]pyrimidine heterocycle core

Mohit Chawla, [ID] *[a] Albert Poater, [ID] [b] Romina Oliva[c] and Luigi Cavallo [ID] *[a]

This study presents a comprehensive theoretical exploration of the fluorescent non-natural emissive nucleobases- ^{mth}A, ^{mth}G, ^{mth}C, and ^{mth}U derived from the methylthieno[3,4-*d*]pyrimidine heterocycle. Our calculations, aligning with experimental findings, reveal that these non-natural bases exert minimal influence on the geometry of classical Watson–Crick base pairs within an RNA duplex, maintaining H-bonding akin to natural bases. In terms of energy, the impact of the modified bases, but for ^{mth}G, is also found to be little significant. We delved into an in-depth analysis of the photophysical properties of these non-natural bases. This investigation unveiled a correlation between their absorption/emission peaks and the substantial impact of the modification on the energy levels of the highest unoccupied molecular orbitals (HOMO) and the lowest unoccupied molecular orbital (LUMO). Notably, this alteration in energy levels resulted in a significant reduction of the HOMO–LUMO gap, from approximately 5.4–5.5 eV in the natural bases, to roughly 3.9–4.7 eV in the modified bases. This shift led to a consequential change in absorption and emission spectra towards longer wavelengths, elucidating their bathochromic shift.

Introduction

In the realm of synthetic biology, a prominent objective involves engineering biological systems to cater to diverse applications.[1–3] One such endeavor revolves around the manipulation of natural nucleobases, traditionally devoid of fluorescence, into fluorescent bases. These modified bases serve as invaluable labeling tags, facilitating the investigation of nucleic acid interactions with various biomolecules.[4] Such approach has already witnessed successful application across a spectrum of biotechnological and biomedical domains.[5–15] Fluorescent nucleobase analogues are utilized for exploring the photophysical properties within duplex and G-quadruplex structures,[16] developing Fluorescent Molecular Rotors (FMRs), which are crucial for investigating nucleic acids structure and function, and designing nucleobase analogs as multiphoton fluorescent probes.[17] Additionally, they play a role in creating antisense oligonucleotide-incorporated fluorescent reporters for live cell imaging.[18]

The ideal engineered fluorescent nucleobases aim for isomorphism with their parent nucleobases while retaining selective base-pairing, thereby ensuring minimal disruption to the structure of nucleic acids. These developments mark significant strides in enabling advanced research and applications within this domain.[13,19,20] Interestingly, the scientific community has documented over a hundred distinct fluorescent nucleobase analogs in literature.[21]

One of the extensively utilized synthetically altered fluorescent nucleobases is 2-aminopurine, akin to natural adenine. This compound exhibits fluorescence both in its singular form and when integrated into duplex DNA in a solution.[22] However, its presence tends to compromise the stability of the DNA duplex structure and prompts mispairing interactions with thymine within the DNA framework.[23] An alternative approach revolves around modifications at the C8 or N7 positions of adenine, involving the incorporation of a triazole functionality. This strategy showcases fluorescent properties while inducing only a moderate destabilization of duplex DNA structures.[24] This avenue of exploration has led to the investigation of various natural base analogs, some commercially available, which display moderate fluorescence upon integration into duplex DNA structures.[20,25–39]

In this context, Tor and colleagues devised two comprehensive sets of fluorescent analogs for RNA nucleosides.

[a] *King Abdullah University of Science and Technology (KAUST), Physical Sciences and Engineering Division, KAUST Catalysis Center, Thuwal 23955-6900, Saudi Arabia. E-mail: mohit.chawla@kaust.edu.sa, luigi.cavallo@kaust.edu.sa*

[b] *Institut de Química Computacional i Catàlisi and Departament de Química, Universitat de Girona, c/Mª Aurèlia Capmany 69, Girona 17003, Catalonia, Spain*

[c] *Department of Sciences and Technologies, University Parthenope of Naples, Centro Direzionale Isola C4, Naples, I-80143, Italy*

16358 | *Phys. Chem. Chem. Phys.*, 2024, **26**, 16358–16368

This journal is © the Owner Societies 2024

These analogs, derived from the thieno[3,4-*d*]-pyrimidine and isothiazolo[4,3-*d*]pyrimidine heterocycle core, form a complete alphabet and are both isomorphic and isofunctional to the natural nucleosides.[20] The first set of synthesized nucleosides based on thieno[3,4-*d*]-pyrimidine core lack the N7 atom of the purine skeleton, whose basicity and coordinating ability is required for many biomolecular interactions.[20] Therefore, these emissive nucleosides were not expected to be fully compatible with the RNA function.

To tackle this challenge and strive toward the objective of creating an emissive alphabet that closely mimics the natural nucleosides in both structure and function, the same authors developed a new generation of nucleosides. This updated set is based on the isothiazolo[4,3-*d*]-pyrimidine heterocyclic core, resulting in ^{tz}A, ^{tz}G, ^{tz}C, and ^{tz}U nucleosides. Notably, this series maintains the N7 atom within the purine skeleton, ensuring structural fidelity while enhancing their emissive properties.[19] Thus, these new emissive nucleosides are isomorphic and possess structural similarity to natural purines, and have been shown to be also 'isofunctional' to natural nucleosides, since the adenosine deaminase is able to deaminate the adenosine analogue ^{mth}A as effectively as the natural adenosine.[40] However, this alphabet is associated with a clear disadvantage deriving from hypochromic shifts and reduced emission quantum yields.

Hence, quite recently, third series of emissive ribonucleoside analogs was developed.[41] This new set is based on the methylthieno[3,4-*d*]-pyrimidine core and was designed to explore the photophysical characteristics of this novel alphabet, see Fig. 1. Intriguingly, these synthesized nucleosides exhibit improved photophysical properties. Despite inducing structural changes at the Hoogsteen edge through the introduction of a methyl group, this updated emissive alphabet holds promise for advancing the biophysical analysis of specific RNA-related processes.[41]

To complement this experimental information, here we performed electronic structure calculations to evaluate the impact of the modification on the structure and energy of the base pairs containing the methylthieno[3,4-*d*]-pyrimidine analogues ^{mth}A, ^{mth}G, ^{mth}C, and ^{mth}U. Following an approach that we have used to evaluate the impact of natural and non-natural modifications on H-bonding base pairing,[42–48] we initially focused on the effect of the modification on the geometry and energetics of the H-bonded base pairs they participate in. Initially, our focus was directed towards the classical *cis* Watson–Crick pairing (*c*WW), given that the Watson–Crick edge remains unaffected across all four modified nucleobases. Additionally, we conducted a comparative assessment of the aromatic characteristics between natural and non-natural nucleobases. This investigation aimed to explore potential effects on their stacking properties, thereby influencing the stability of the encompassing nucleic acid structure. Furthermore, we used time-dependent density functional theory (TD-DFT), already successfully employed in literature for similar applications,[16,49–52] to analyze the impact of these modifications on the UV-Vis properties of natural nucleosides and to calculate the optical absorption properties of both modified nucleobases and nucleosides. These findings were then rationalized in terms of alterations in the molecular orbitals caused by the modifications.

Models and computational details

To investigate the geometry and stability of the non-natural modified base pairs under examination, we conducted modeling of the H-bonded modified base pairs. This involved employing density functional theory (DFT) and post Hartree–Fock methods to calculate their binding energy. To allow straightforward comparison with results previously published, we performed the calculations at exactly the same level of theory.

Modeling the non-natural base pairs

We first study the impact on H-bonding of the non-natural ^{mth}A, ^{mth}G, ^{mth}U, and ^{mth}C bases forming classical Watson–Crick base pairs in combination with the classical A, G, C, and
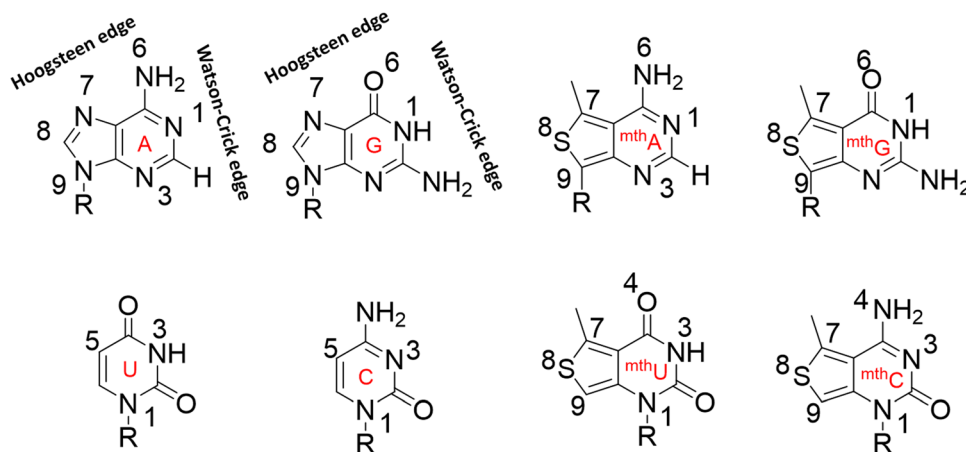

Fig. 1 Structures of the natural (A/G/U/C) and fluorescent nucleobases (^{mth}A/^{mth}G/^{mth}U/^{mth}C). The sugar–phosphate backbone of the natural and non-natural bases has been truncated at C1′, notated as 'R' in the figure.

This journal is © the Owner Societies 2024

Phys. Chem. Chem. Phys., 2024, **26**, 16358–16368 | **16359**

U bases, by taking into account the ^{mth}A:U, A:^{mth}U, ^{mth}G:C, and G:^{mth}C base pairs. Further, we also modeled the H-bonding interactions where both the bases were modified, that is the ^{mth}A:^{mth}U and ^{mth}G:^{mth}C base pairs. In addition, we also modeled the canonical A:U and G:C base pair geometries as well for the sake of comparative analysis. Thus, in total, we modeled eight different combinations of the non-natural modified base pair systems along with their natural base pair counterparts. For all the model systems described above, the base pairs are truncated at the C1′ atom of the ribose. This is the standard approach used in literature.[43,44,47,53–56]

QM calculations of the modeled base pairs

Geometry optimizations were performed within a DFT approach, based on the hybrid B3LYP functional as implemented in the Gaussian 09 package.[57–59] The correlation-consistent polarized valence triple-ζ cc-pvTZ basis set[60] was used for all the geometry optimizations in gas phase as well as in water, modeled with the C-PCM continuum solvation model.[61] As dispersion interactions could impact the stability of the examined base pairs in varying degrees, we included the Grimme D3 correction term with the Becke–Johnson damping scheme to account for these contributions to the electronic energy.[62] Interaction energies were calculated on the B3LYP-D3/cc-pvTZ optimized geometries at the second order Møller–Plesset (MP2)[63] level of theory using the augmented aug-cc-pvTZ basis set. For these calculations we took advantage of the faster RIMP2[64] method as implemented in Turbomole 6.1 package, with water modeled with the continuum solvation model COSMO.[61] All the interaction energies were corrected for the basis set super position error (BSSE),[65] using the counterpoise procedure.[65] Thus, the binding energy E_{Bind} is calculated as in eqn (1):

$$E_{Bind} = E_{Complex} - (E_{M1} + E_{M2}) + BSSE; \quad (1)$$

where $E_{Complex}$ is the electronic energies of the optimized M1:M2 base pair, and E_{M1} and E_{M2} are the electronic energy of the isolated geometries of the M1 and M2 bases, and BSSE is the basis set superposition error calculated as proposed by Boys and Bernardi.[65] Within this approach, the deformation energy, which is the energy required to deform the bases from the isolated geometry to the geometry they have in the base pair, is included in our calculations. This is a rather standard approach used in this kind of calculations.[44,47,53–55,66,67] In the present study, we also derived the interaction energies in water, which were calculated using the same recipe as suggested by Sponer and coworkers.[53,68] However, it is recognized that "in-water" calculations are inherently less accurate than gas-phase calculations.[69] Despite this, "in water" calculations using COSMO are valuable for describing the perturbation of the electrostatic field of solute molecules by the polar solvent and the coulombic interaction between solute and solvent. This method provides a reasonable assessment of bulk solvent screening of the electrostatic contribution to base pairing, especially when considering relative trends. Therefore, in this

study, we discuss both gas-phase and "in water" COSMO calculations.

To have an immediate and intuitive understanding of the impact of a specific modification, we introduced the modification energy, E_{Mod}, defined as the energy difference between the binding energy of the modified and of the corresponding natural base pair (in this specific case A:U and G:C base pair),[42,43,70,71] as shown in eqn (2).

$$E_{Mod} = E_{Bind} \text{ (modified base pair)} - E_{Bind} \text{ (natural base pair).} \quad (2)$$

Within this definition, positive and negative E_{Mod} values indicate modifications that decrease or increase the stability of a specific base pair, respectively.

Absorption and emission spectra were calculated using time dependent density functional theory (TD-DFT),[72–74] with the B3LYP functional as implemented in the Gaussian09 package. A similar approach has already been performed on the non-natural emissive nucleobases derived from thieno[3,4-d]-pyrimidine heterocycle and isothiazolo[4,3-d]-pyrimidine heterocycle core.[75,76] Geometry optimization of the singlet ground state S_0 (for adsorption) and of the first singlet excited state S_1 (for emission) were performed without symmetry constraints. For the absorption peaks, we always assumed a transition between the single ground state and the first excited singlet state. To facilitate a comparison between the predicted absorption and emission wavelengths and experimental findings, we incorporated water as an implicit solvent in our calculations.

Electron density analysis

Comparative analysis of the electron density of natural (A/U/G/C) and modified (^{mth}A, ^{mth}U, ^{mth}G, ^{mth}C) bases was performed as follows. For example, first, the geometry of the ^{mth}A base was optimized at the B3LYP/cc-pvTZ level of theory. For the sake of easier analysis, C_S symmetry with the symmetry plane coincident with the purine plane was imposed, and the electron density analysis was performed in the symmetry plane. After optimization, we compared the RI-MP2/aug-cc-pvTZ electron densities of the modified ^{mth}A base, ρ^{mthA}, and that of the unmodified A base with the geometry it has in the ^{mth}A base, $\rho^{A/mthA}$. In other words, we took the optimized geometry of the ^{mth}A base, and we replaced the C9 carbon of ^{mth}A with nitrogen, plus we replaced the S8 atom of ^{mth}A with a carbon, further, we replaced the C7 atom in ^{mth}A with N atom and replaced the methyl group with a hydrogen atom. The geometry of this natural and non-modified A base was optimized by fixing the atoms of the 6-membered ring that is common among the modified ^{mth}A and the natural A base. With this approach, the heavy atom skeleton of the ^{mth}A and A bases is identical and can be perfectly superimposed. This is fundamental to avoid noise in the analysis of the electron density difference, $\rho^{mthA-A/mthA} = \rho^{mthA} - \rho^{A/mthA}$. A similar procedure was followed for the other bases.

Aromaticity analysis

Aromaticity of the nucleobases was quantified using the nucleus-independent chemical shifts (NICS) values proposed

16360 | *Phys. Chem. Chem. Phys.*, 2024, **26**, 16358–16368

This journal is © the Owner Societies 2024

by Schleyer and co-workers,[77] computed using the gauge-including atomic orbital method[78] (GIAO) and including the solvent contribution by C-PCM. The NICS is defined as the negative of the absolute shielding computed at specific points around the molecular system, in particular at ring centres, NICS(0) values, or d Å above such ring centres, NICS(d) values.[79] In the current work, NICS(1) is defined as the average value of the shielding calculated 1 Å above and below the plane of the overall planar bases.

Results and discussion

To investigate the influence of the fluorescent modified nucleo-bases (^{mth}A, ^{mth}U, ^{mth}G, and ^{mth}C) on the structure and stability of nucleic acid base pairs, we examined eight distinct base pairs characterized by a classical antiparallel Watson–Crick (cWW) geometry typical of duplex structures. The optimized geometry and binding energies were calculated for these base pairs in both the gas phase and aqueous environments. Similarly to our previous studies,[75,76] in this work we have calculated the modification energy, E_{Mod}, defined as the difference between the binding energy of the modified and of the corresponding unmodified base pair, for instance cWW ^{mth}A:U or cWW ^{mth}A:^{mth}U vs. cWW A:U (see Methods), which will give an immediate effect of the impact of specific modification on the base pair. Negative and positive E_{Mod} values delineate whether the modified base pair exhibits greater or lesser stability than its unmodified counterpart. Table 1 compiles the calculated interaction energies and E_{Mod} values for the analyzed base pairs. Additionally, Fig. 2 illustrates the optimal geometries of the base pairs forming 'Watson–Crick' arrangements, showcasing H-bonding distances in both gas phase and in water.

Structure and energy impact of the modified nucleobases on H-bonded base pairs

Eight cWW base pairs were considered, four related to the A:U and four to the G:C pair, namely the unmodified A:U and G:C cWW and the fully modified ^{mth}A:^{mth}U and ^{mth}G:^{mth}C pairs, along with the base pairs hosting a single modified base,

i.e. ^{mth}A:U/A:^{mth}U and ^{mth}G:C/G:^{mth}C (see Fig. 2). The optimized structure of the modified ^{mth}A:U, A:^{mth}U and ^{mth}A:^{mth}U cWW base pairs is extremely similar to that of the classical A:U cWW pair, with differences in H-bond lengths within 0.02 Å. Similarly, the C1′–C1′ distances (which gives an indication of the isostericity of H-bonded base pairs)[80,81] are almost identical in the modified and unmodified A:U pairs (10.52 Å for A:U versus 10.51/10.49/10.48 Å for A:^{mth}U/^{mth}A:U/^{mth}A:^{mth}U). An analogous trend is observed for base pairs involving the ^{mth}G and ^{mth}C modifications. The geometry of ^{mth}G:C, G:^{mth}C, and ^{mth}G:^{mth}C base pairs closely mirrors that of the natural G:C cWW base pair, with differences in H-bond distances within 0.04 Å. Likewise, the C1′–C1′ distances are very similar (10.71 Å for G:C versus 10.78/10.78/10.79 Å for G:^{mth}C/^{mth}G:C/^{mth}G:^{mth}C).

The binding energy of the modified pairs involving ^{mth}A and ^{mth}U bases have a slight destabilizing effect with an E_{Mod} of 0.67/025 kcal mol^{-1} for cWW A:^{mth}U base pair in gas phase/water. This can be attributed to the decreased electron density around the N3 atom of ^{mth}U, making it a less effective donor compared to the canonical U base (Fig. 3). Conversely, a slight stabilization is observed for ^{mth}A:U, with an E_{Mod} of -0.59/-0.47 kcal mol^{-1} in gas phase/water, respectively. This stabilization is attributed to a slight increase in electron density around N6 of ^{mth}A, making it a better H-bond donor, and N1 of ^{mth}A, a superior H-bond acceptor, explaining a stabilization effect of ^{mth}A:U compared to canonical A:U base pair.

In contrast, the modified base pairs involving ^{mth}G exhibit a significant destabilizing effect, with E_{Mod} values ranging from +3.26/+0.61 to +2.35/+0.29 kcal mol^{-1} for ^{mth}G:C and ^{mth}G:^{mth}C in gas phase/water, respectively. Electron density difference analysis reveals that the O6 of ^{mth}G has increased electron density, while N1 of ^{mth}G becomes a poor H-bond donor, leading to an overall less stable base pair compared to the canonical G:C pair (Fig. 3). For G:^{mth}C pairs, a slight stabilization effect of -0.77/-0.51 kcal mol^{-1} is observed, attributed to the enhanced electron density around O2 and N4 of ^{mth}C, making them better H-bond acceptors and donors, respectively, compared to the canonical G:C base pair.

In conclusion, our analysis confirms the absence of deformation or strain in RNA duplexes due to modified bases.

Table 1 Energy decomposition values, measured in kcal mol^{-1}, for cWW geometries of both modified and corresponding natural bases. E_{Int} represents the interaction energy of the base pair, excluding deformation energy. E_{def} signifies the deformation energy calculated as the difference between the energy of the base pair's geometry and the energy of each base's geometry when optimized individually. E_{Bind} is the summation of interaction and deformation energies ($E_{Bind} = E_{Int} + E_{Def}$). E_{mod} reflects the difference between the binding energy of the modified base pair and the reference pair (A:U and G:C). Negative or positive values of E_{Mod} indicate whether the modified base pair is more or less stable compared to the corresponding unmodified pair. These energy values were computed using the RI-MP2/aug-cc-pVTZ//B3LYP/cc-pVTZ level of theory

System	Geometry	E_{Int}	E_{Def}	E_{Bind} (gas)	E_{mod} (gas)	E_{Bind} (water)	E_{mod} (water)
A:U	cWW	−16.51	1.50	−15.01	—	−7.93	—
A:^{mth}U	cWW	−15.73	1.38	−14.34	0.67	−7.69	0.25
^{mth}A:U	cWW	−17.37	1.77	−15.60	−0.59	−8.41	−0.47
^{mth}A:^{mth}U	cWW	−16.42	1.64	−14.78	0.23	−8.12	−0.19
G:C	cWW	−30.74	2.75	−27.99	—	−12.49	—
G:^{mth}C	cWW	−32.10	3.34	−28.76	−0.77	−13.00	−0.51
^{mth}G:C	cWW	−28.04	3.32	−24.72	3.26	−11.89	0.61
^{mth}G:^{mth}C	cWW	−28.87	3.23	−25.64	2.35	−12.21	0.29

This journal is © the Owner Societies 2024

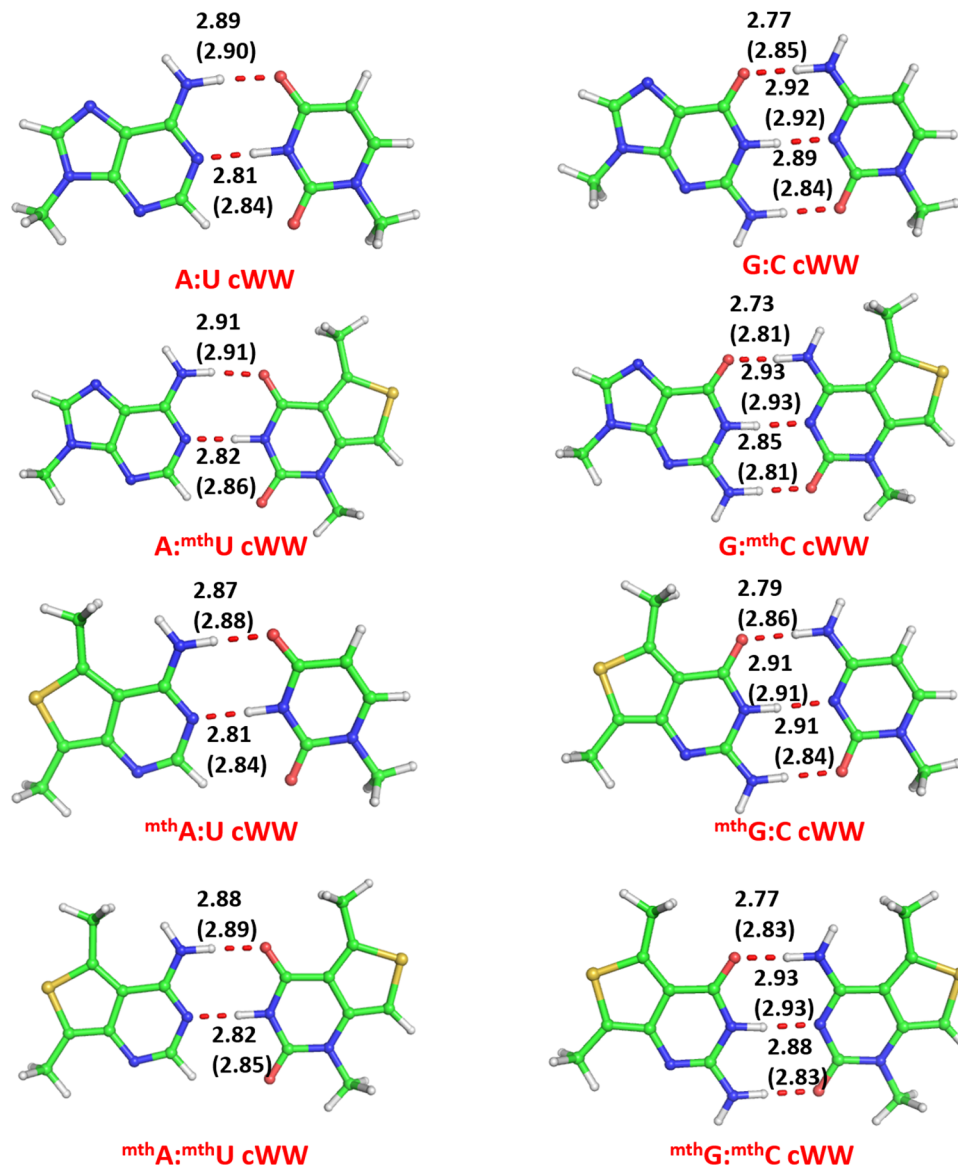Phys. Chem. Chem. Phys., 2024, **26**, 16358–16368 | **16361**

Fig. 2 *Cis* Watson−Crick base pairs. Stick representation of unmodified and modified *c*WW A:U base pairs (left) and of unmodified and modified *c*WW G:C base pairs (right). Values in parentheses correspond to optimized H-bond distances in water and values out of parentheses correspond to optimized distances in the gas phase. All distances are in Å.

They maintain indeed an H-bonding geometry comparable to that of the natural bases.

Nevertheless, we observe a specific destabilization trend in base pairs containing the ^{mth}G modification, particularly pronounced in gas phase calculations. This warrants further investigation, particularly within the context of complex RNA structures.

Aromaticity analysis

To assess the impact of aromaticity on the 6 and 5-membered rings in the non-natural methylthieno bases in comparison to their natural counterparts, we utilized the nucleus-independent chemical shift (NICS) as a metric.[77] The NICS is defined as the negative of the absolute shielding calculated at specific points within the molecular system, specifically at the ring centers, known as NICS(0) values, or at positions 1 Å above the ring centers, referred to as NICS(1) values.[79] Larger NICS values, *i.e.*, more negative values, indicate a higher level of ring aromaticity. In these computations, the NICS values of benzene served as the reference point. The data presented in Table 2 highlights a consistent trend: the NICS index for the 6-membered ring consistently shows lower values compared to benzene. This suggests a reduced level of aromaticity within the 6-membered ring, observed in both natural and non-natural bases.

Comparing the NICS(1) indices between natural and non-natural bases, we observe a further decrease in aromaticity of the 6-membered ring in purine and pyrimidine bases for the non-natural variants. For instance, the NICS(1) value for the 6-membered ring of ^{mth}A is only −6.06, while it is −8.01 for A. This sharp decrease in aromaticity is notable in the non-natural base.

16362 | *Phys. Chem. Chem. Phys.*, 2024, **26**, 16358–16368

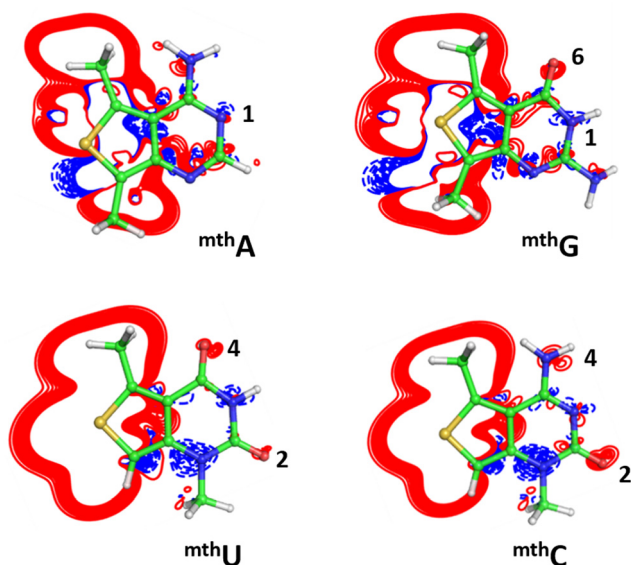This journal is © the Owner Societies 2024

Fig. 3 Electron density maps. Electron density differences, in the base plane, between modified and unmodified bases are shown on the structures of the four modified bases, ^{mth}A, ^{mth}G, ^{mth}C and ^{mth}U. Density difference curves are plotted between −0.02 and 0.02 a.u., with a spacing of 0.001 a.u. blue (red) lines refer to negative (positive) density difference curves, *i.e.*, to areas where the modified base presents reduced (increased) electron density, as compared to the corresponding natural base.

Table 2 NICS(0), NICS(1) and HOMA aromaticity values for natural and modified bases

	6 membered ring			5 membered ring	
	NICS(0)	NICS(1)	HOMA	NICS(0)	NICS(1)
C_6H_6	−8.227	−10.370	0.995	—	—
A	−6.032	−8.006	0.978	−11.201	−9.709
^{mth}A	−2.246	−5.380	−0.693	−13.475	−11.059
C	−1.347	−3.173	0.755	—	—
^{mth}C	0.320	−2.041	−0.563	−12.577	−9.276
G	−2.909	−3.426	0.803	−10.611	−8.821
^{mth}G	−0.046	−1.864	−0.523	−11.848	−9.240
U	−1.089	−1.786	0.640	—	—
^{mth}U	0.150	−0.891	−0.533	−12.332	−9.050

This trend is consistent across the other bases. Conversely, the aromaticity of the 5-membered ring of non-natural purines ^{mth}A/^{mth}G, is higher, where the C8–H group in the natural base

is replaced by a S8, and N7 is replaced with C–CH$_3$. Specifically, the NICS(1) of the 5-membered ring of ^{mth}A is −11.63, compared to −9.71 for A. A similar trend is observed for ^{mth}G and G. In summary, this analysis indicates that in the 6-membered ring of non-natural bases, the delocalization of electrons in the π-conjugated aromatic system is less extensive compared to natural nucleobases. Conversely, electron delocalization is more pronounced in the 5-membered ring of non-natural purines compared to natural purines.

To corroborate the findings from the NICS comparison, the harmonic oscillator model of aromaticity (HOMA), which is defined as the normalized sum of squared deviations of bond lengths from the optimal value in benzene, was also calculated, as shown in Table 2. This alternative analysis further supports the decrease in aromaticity of the 6-membered ring in the non-natural ^{mth}A, ^{mth}U, ^{mth}G, and ^{mth}C bases, when compared to the natural A, U, G and C bases. Interestingly, the substitution in the unnatural bases in the additional 7 position, with respect to the results of our previous studies imposes an additional destabilization of both rings of different size[75] reducing the NICS values by an amount significant but never higher than 0.1 units in the case of the 6-membered ring, but already more pronounced up to 1.5 units in the 5-membered ring. Therefore, the 5-membered ring has greater aromaticity if there is a N atom in the ring, rather than a C–CH$_3$ group. Furthermore, the reduction in aromaticity is more pronounced for the ^{mth}U and ^{mth}G bases. This is due to the repulsion between two pairs of hydrogen atoms that are placed at 2.223, 2.169 Å for the bases ^{mth}A and ^{mth}C between the C–CH$_3$ group and one hydrogen of the NH$_2$ group since the whole group is placed in the same plane of the 6-membered ring. While there are attractive H-bonds of those two hydrogens of the methyl fragment C–CH$_3$ and the oxygen of the keto group of the 6-membered ring of ^{mth}G and ^{mth}U, but at a relatively long distance of 2.856 and 2.818 Å. In addition, these interactions are relevant between the hydrogen atoms of the C–CH$_3$ group of the 5-membered ring with the NH$_2$ or the O moieties of the 6-membered ring because the decrease in aromaticity is more pronounced for in NICS(1) instead of NICS(0) due to the hydrogen atoms of the C–CH$_3$ group lying out of the plane of the rings.

To assess the potential changes in the aromaticity of bases upon the formation of base pairs, we computed the NICS (1) for individual bases when incorporated into base pairs. Analysis of

Table 3 NICS(1) values for the base pairs: A:^{mth}U, ^{mth}A:^{mth}U, ^{mth}A:U, G:^{mth}C, ^{mth}G:^{mth}C, ^{mth}G:C (between parentheses the differences with respect to the single bases in Table 2)

	Base left		Base right	
	6 membered ring	5 membered ring	6 membered ring	5 membered ring
A:U	−7.417 (−0.589)	−9.618 (−0.091)	−1.750 (−0.036)	—
A:^{mth}U	−7.380 (−0.626)	−9.550 (−0.159)	−0.942 (−0.922)	−8.962 (−0.088)
^{mth}A:^{mth}U	−4.717 (−0.663)	−10.736 (−0.323)	−0.962 (−0.902)	−9.010 (−0.040)
^{mth}A:U	−4.689 (−0.691)	−10.809 (−0.250)	−1.803 (0.017)	—
G:C	−3.519 (0.093)	−8.704 (−0.117)	−2.677 (−0.496)	—
G:^{mth}C	−3.492 (0.066)	−8.559 (−0.262)	−1.770 (−0.271)	−10.387 (1.111)
^{mth}G:^{mth}C	−2.037 (0.173)	−9.109 (−0.131)	−1.783 (−0.258)	−9.344 (0.068)
^{mth}G:C	−2.057 (0.193)	−9.070 (−0.170)	−2.755 (−0.418)	—

This journal is © the Owner Societies 2024

Phys. Chem. Chem. Phys., 2024, **26**, 16358–16368 | **16363**

Table 3 indicates a clear trend where the aromaticity values closely resemble those of isolated bases. However, a subtle elevation in aromaticity is observed, averaging approximately 0.5 ppm, and reaching up to 1 ppm in agreement with our prior studies.[75] It should be noted that it is the ^{mth}U base that sees its aromaticity most altered, and even more the ^{mth}C base in G:^{mth}C, but only up to a loss of aromaticity of 1.111 ppm.

Photophysical properties of methylthieno[3,4-*d*]-pyrimidine nucleobase analogues

Time-dependent density functional theory (TD-DFT) has emerged as a highly reliable technique for predicting properties such as absorption, emission, quantum yield, and transition dipole moment, in previous studies where various fluorescent base analogues were characterized as monomers, as well as inside RNA and/or DNA strands. It has also proven instrumental in the rational design of fluorescent nucleobase analogues. For example, TD-DFT calculations conducted on nine quadracyclic adenine derivatives successfully described their relative fluorescence quantum yield and brightness, indicating the potential for employing a TD-DFT-based rational design strategy to develop bright fluorophores from a common scaffold, thereby streamlining the otherwise costly and time-consuming screening process.[52] In a subsequent study by the same authors, TD-DFT calculations were utilized to predict the transition dipole moment orientation for qAN4 and qAnitro bases, revealing an associated phase angle of 25 degrees.[51] Additionally, the fluorescent base analogue *t*CO was successfully incorporated into RNA, maintaining the A-form duplex structure, enhancing stability, and exhibiting high fluorescence quantum yield, positioning it as a potentially valuable fluorescent RNA base analogue with superior brightness compared to existing internal RNA analogues.[50] Additionally, Manderville, Wetmore, and their team investigated fluorescent donor–acceptor (D–A) 8-aryl-dG probes incorporated within the thrombin

binding aptamer (TBA), impacting the stability of G-quadruplex (GQ) structures. These probes, which feature diverse moieties, demonstrate potential in distinguishing between duplex and GQ configurations, thus facilitating fluorescence-based applications such as molecular sensing and diagnostics. Their ability to be selectively excited and their sensitivity to environmental conditions position them as promising tools for monitoring molecular interactions and structural changes.[16]

In this study, we also used the TD-DFT studies to calculate the photophysical properties of natural and non-natural fluorescent nucleobases, see Table 4, since our previous studies showed that TD-DFT reproduces the absorption/emission peaks better than the RI-CC2 approach.[75,76] Calculating the energy difference between the ground (S_0) and the first excited singlet state (S_1), we find the energy absorption peaks at 354, 333, 333 and 302 nm for ^{mth}A, ^{mth}G, ^{mth}C and ^{mth}U, respectively, which are in good agreement with the experimentally reported absorption peaks of 353, 327, 323 and 316 nm.[41] We report all the peaks using TD-DFT in the present work. Although S_0 and S_1 involve contributions from neighbor orbitals, peaks are dominated by the π to π^* HOMO to LUMO transition. For comparison, we also calculated the same absorption peaks for the natural nucleobases, 251, 248, 256 and 246 nm for A, G, C and U bases, which compare with experimental values of 259, 252, 271, and 262 nm, respectively.[82] This indicates that the methylthieno[3,4-*d*]-pyrimidine modification results in a bathochromic shift of roughly 102/90 nm for ^{mth}G/^{mth}A, and of roughly 80/58 nm for ^{mth}C/^{mth}U, as compared to their natural counterparts. Slightly larger bathochromic shifts were calculated in the emission spectra,[83] with bathochromic displacements of 160, 158, 143 and 109 nm for ^{mth}A,

Table 4 In the first columns, predicted photophysical properties (wavelength and oscillator strength), as calculated by TD-DFT are reported (values in parentheses are the corresponding experimental values[19]). In the last columns, HOMO (H), LUMO (L) and HOMO−LUMO gap energies (ΔE_{HL}) are reported. For the sake of comparison, all the values were calculated and are reported for the methylthieno[3,4-*d*]-pyrimidine nucleobase analogues, for the thieno[3,4-*d*]-pyrimidine bases and for the natural bases

Base	Absorption		Emission		H	L	ΔE_{HL}
	λ_{abs}	os. str.	λ_{em}	os. str.			
^{mth}A	353.9 (353)	0.168	462.6 (467)	0.195	−5.76	−1.82	−3.94
^{mth}G	332.7 (327)	0.109	451.7 (456)	0.126	−5.96	−1.64	−4.32
^{mth}C	332.7 (323)	0.093	465.4 (455)	0.103	−6.10	−1.88	−4.22
^{mth}U	301.6 (306)	0.071	393.4 (427)	0.094	−6.54	−1.81	−4.73
^{th}A	343.7 (341)	0.177	434.2 (420)	0.219	−6.05	−1.97	−4.08
^{th}G	329.9 (321)	0.111	433.2 (453)	0.134	−6.02	−1.72	−4.30
^{th}C	329.7 (320)	0.095	439.6 (429)	0.119	−6.19	−1.87	−4.32
^{th}U	299.3 (304)	0.073	374.4 (409)	0.106	−6.57	−1.85	−4.72
A	251.5	0.268	302.86	0.467	−6.29	−0.91	−5.38
G	252.8	0.128	293.50	0.103	−6.25	−0.79	−5.46
C	252.9	0.197	321.97	0.202	−6.68	−1.23	−5.45
U	243.6	0.185	284.26	0.271	−7.14	−1.61	−5.53

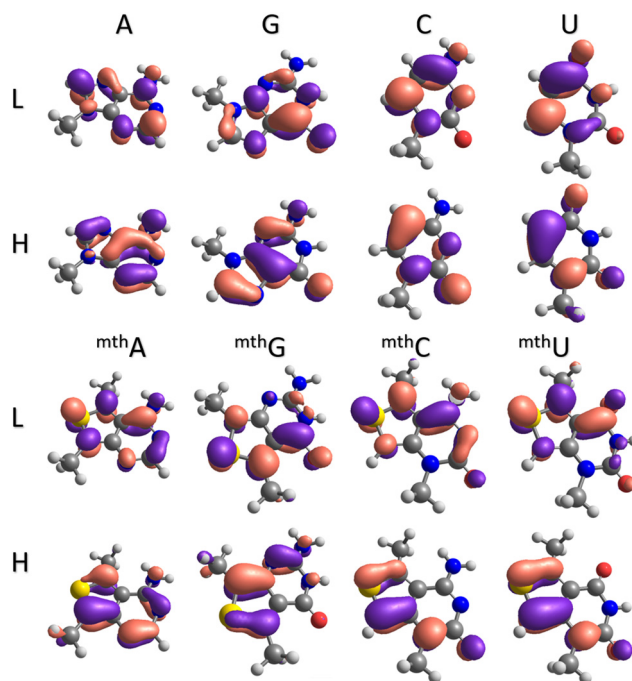**Fig. 4** Graphic representation of the frontier molecular orbitals of the natural bases (top) and the modified ones (bottom).

16364 | *Phys. Chem. Chem. Phys.*, 2024, **26**, 16358–16368

This journal is © the Owner Societies 2024

^{mth}G, ^{mth}C and ^{mth}U with respect to natural bases. We find the energy emission peaks at 463, 452, 465 and 393 nm for ^{mth}A, ^{mth}G, ^{mth}C and ^{mth}U, respectively, which are in good agreement with the experimentally reported peaks of 467, 456, 455 and 427 nm. For the sake of comparison, we calculated here the absorption/emission peaks also for first generation non-natural alphabet proposed by Tor and co-workers,[75,76] thA, thG, thU, thC. As compared to thA, thG, thU, thC, the third generation ^{mth}A, ^{mth}G, ^{mth}C and ^{mth}U, analysed here, also exhibited a batochromic shift, by 10, 3, 3, 2 nm, respectively, for absorption, and by 28, 18, 26, 19 nm, respectively, for emission.[41]

As expected, and in light of the above results, the HOMO and LUMO play a major role in the absorption/emission properties of the bases featuring the methylthieno[3,4-d]-pyrimidine modification, therefore we decided to further analyse how the above modification impacts these orbitals. Previously, we had shown a clear correlation between the bathochromic shifts of the tz- and ts-bases and the HOMO to LUMO energy gap.[75,76]

Data reported in Table 4 shows that the energy of both the HOMO and LUMO is substantially altered by the modification, with differences between a non-natural base and its natural analogue within roughly 0.29–0.58 eV for HOMO and 0.37–0.91 for LUMO. This reduces the HOMO–LUMO gap from roughly 5.4–5.5 eV in the natural bases to roughly 3.9–4.7 eV in the modified methylthieno[3,4-d]-pyrimidine bases, with the consequent bathochromic shift in the absorption and emission spectra. Considering that both the HOMO and LUMO energies are substantially changed from the natural bases, we report their shapes in Fig. 4. As illustrative examples, the LUMOs of A, G, C and U are compared to those of the homologous
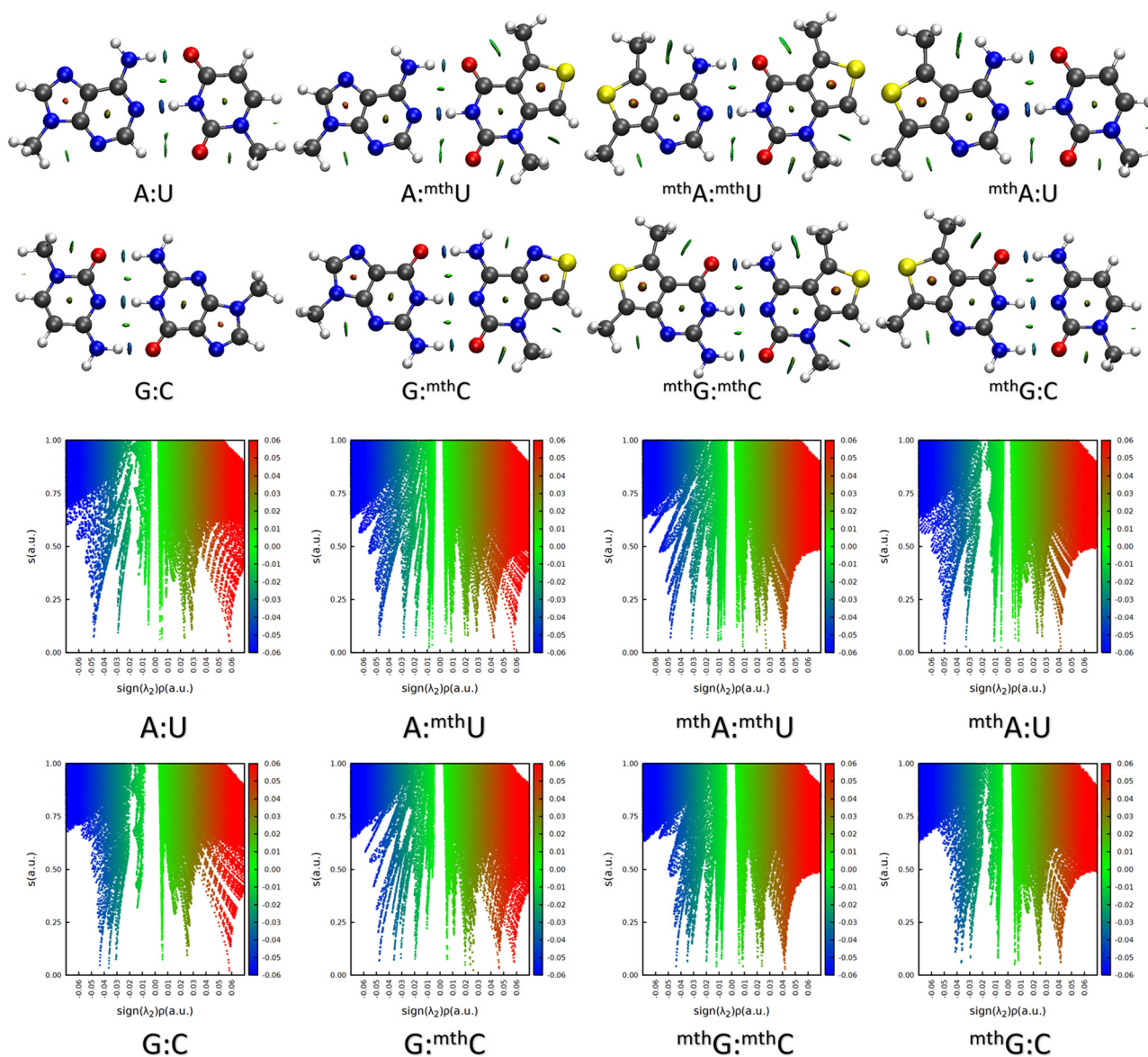

Fig. 5 NCI plots of the base pairs: A:U, A:^{mth}U, ^{mth}A:^{mth}U, ^{mth}A:U, G:C; G:^{mth}C, ^{mth}G:^{mth}C and ^{mth}G:C. The isosurface represents a value of 0.5 with a color scale for the reduced density gradient (above the 3D representation and below the 2D representation).

This journal is © the Owner Societies 2024

Phys. Chem. Chem. Phys., 2024, **26**, 16358–16368 | **16365**

modified ^{mth}A, ^{mth}G, ^{mth}C and ^{mth}U in Fig. 4. Inspection of the shape of the HOMO of the modified bases shows higher participation of the 5-membered ring for the ^{mth}G base, with a strong participation of the S8 atom with its low energy π orbitals, which destabilize the HOMO. Since the LUMO is also stabilized, less quantitatively than the destabilization of the HOMO, the HOMO–LUMO gap reduces significantly, and thus, the stability of the modified bases decreases. Finally, the reduced bathochromic shift of modified pyrimidines can also be rationalized in terms of reduced aromaticity of modified and natural pyrimidines relative to purines, see Table 2, which lowers the impact of the S8 atom on the absorption/emission properties of the modified bases. In addition, we calculated the non-covalent interaction (NCI) plots,[84,85] to determine whether the greater or lesser stability of the base pairs was due to base modification. As can be seen in Fig. 5, these analyses allow us to conclude that the non-covalent interaction between the natural and non-natural pairs do not differ qualitatively. Even though the interaction between the base pairs seems to be identical according to the 3D NCI plots in Fig. 5, this intermolecular interaction means a weakening of the intramolecular H-bonds as can be seen in the 2D NCI plots Fig. 5, particularly for A:^{mth}U and also for the ^{mth}G;^{mth}C and ^{mth}G:C pairs. Oppositely, the favourable interactions are especially important for the ^{mth}A:U, and even more for and G:^{mth}C, in perfect agreement with results in Table 1.

Conclusions

Our investigation delved into the electronic properties and the influence on base-pair stability of a novel emissive RNA alphabet founded on methylthieno[3,4-d]-pyrimidine (^{mth}A, ^{mth}U, ^{mth}G, and ^{mth}C), proposed as highly isomorphic and isofunctional counterparts to the natural nucleobases. Our study demonstrated that these emissive nucleobases exert minimal effects on the geometry of classical Watson–Crick base pairs, suggesting that RNA duplexes can be capable to accommodate them, especially the purine derivatives, without significant alterations in H-bonding. However, the introduction of ^{mth}G in particular may impact their stability. The potential steric implications of the additional methylthieno ring in pyrimidine derivatives also warrant further investigation.

As the stacking interactions play a significant role in the structural stability of nucleic acids, we evaluated the aromaticity of both non-natural emissive and natural nucleobases. Our analysis revealed a subtle reduction in the aromaticity of the 6-membered ring of emissive purines and pyrimidines as compared to their natural counterparts. In contrast, non-natural purines (^{mth}A/^{mth}G) exhibited a significant increase in aromaticity in the 5-membered ring, attributed to the presence of the S8 substitution. The influence of this modified aromaticity on relative stacking interactions would need to be further inquired. Moreover, our assessment of molecular orbitals facilitated a rationalization of the absorption and emission properties of the modified nucleobases, accounting for their fluorescence.

Conflicts of interest

There are no conflicts to declare.

Acknowledgements

References

1 S. A. Benner and A. M. Sismour, *Nat. Rev. Genet.*, 2005, **6**, 533–543.
2 S. A. Benner, *Chimia*, 1987, **41**, 142–148.
3 J. W. Szostak, D. P. Bartel and P. L. Luisi, *Nature*, 2001, **409**, 387–390.
4 W. Liu, D. Shin, Y. Tor and B. S. Cooperman, *ACS Chem. Biol.*, 2013, **8**, 2017–2023.
5 S. G. Srivatsan, N. J. Greco and Y. Tor, *Angew. Chem., Int. Ed.*, 2008, **47**, 6661–6665.
6 S. G. Srivatsan and Y. Tor, *Tetrahedron*, 2007, **63**, 3601–3607.
7 S. G. Srivatsan and Y. Tor, *Nat. Protoc.*, 2007, **2**, 1547–1555.
8 S. G. Srivatsan and Y. Tor, *J. Am. Chem. Soc.*, 2007, **129**, 2044–2053.
9 S. G. Srivatsan, H. Weizman and Y. Tor, *Org. Biomol. Chem.*, 2008, **6**, 1334–1338.
10 N. J. Greco and Y. Tor, *J. Am. Chem. Soc.*, 2005, **127**, 10784–10785.
11 N. J. Greco and Y. Tor, *Nat. Protoc.*, 2007, **2**, 305–316.
12 R. W. Sinkeldam, N. J. Greco and Y. Tor, *Chem. Rev.*, 2010, **110**, 2579–2619.
13 R. W. Sinkeldam, P. A. Hopkins and Y. Tor, *Chem. Phys. Chem.*, 2012, **13**, 3350–3356.
14 R. W. Sinkeldam, L. S. McCoy, D. Shin and Y. Tor, *Angew. Chem., Int. Ed.*, 2013, **52**, 14026–14030.
15 L. M. Wilhelmsson, *Q. Rev. Biophys.*, 2010, **43**, 159–183.
16 D. J. M. Blanchard, K. L. Fadock, M. Sproviero, P. S. Deore, T. Z. Cservenyi, R. A. Manderville, P. Sharma and S. D. Wetmore, *J. Mater. Chem. C*, 2016, **4**, 2915–2924.

16366 | *Phys. Chem. Chem. Phys.*, 2024, **26**, 16358–16368

This journal is © the Owner Societies 2024

17 R. E. Johnson, M. T. Murray, L. J. Bycraft, S. D. Wetmore and R. A. Manderville, *Chem. Sci.*, 2023, **14**, 4832–4844.

18 J. R. Nilsson, C. Benitez-Martin, H. G. Sansom, P. Pfeiffer, T. Baladi, H. N. Le, A. Dahlén, S. W. Magennis and L. M. Wilhelmsson, *PCCP*, 2023, **25**, 20218–20224.

19 A. R. Rovira, A. Fin and Y. Tor, *J. Am. Chem. Soc.*, 2015, **137**, 14602–14605.

20 D. Shin, R. W. Sinkeldam and Y. Tor, *J. Am. Chem. Soc.*, 2011, **133**, 14912–14915.

21 W. Xu, K. M. Chan and E. T. Kool, *Nat. Chem.*, 2017, **9**, 1043–1055.

22 D. C. Ward, E. Reich and L. Stryer, *J. Biol. Chem.*, 1969, **244**, 1228–1237.

23 D. Xu, K. O. Evans and T. M. Nordlund, *Biochemistry*, 1994, **33**, 9592–9599.

24 C. Dyrager, K. Borjesson, P. Diner, A. Elf, B. Albinsson, L. M. Wilhelmsson and M. Grotli, *Eur. J. Org. Chem.*, 2009, 1515–1521, DOI: 10.1002/ejoc.200900018.

25 M. E. Hawkins, *Cell Biochem. Biophys.*, 2001, **34**, 257–281.

26 M. E. Hawkins, W. Pfleiderer, F. M. Balis, D. Porter and J. R. Knutson, *Anal. Biochem.*, 1997, **244**, 86–95.

27 A. R. Hernandez and E. T. Kool, *Org. Lett.*, 2011, **13**, 676–679.

28 A. R. Hernandez, L. W. Peterson and E. T. Kool, *ACS Chem. Biol.*, 2012, **7**, 1454–1461.

29 A. T. Krueger and E. T. Kool, *J. Am. Chem. Soc.*, 2008, **130**, 3989–3999.

30 A. H. Lee and E. T. Kool, *J. Am. Chem. Soc.*, 2006, **128**, 9219–9230.

31 C. Liu and C. T. Martin, *J. Mol. Biol.*, 2001, **308**, 465–475.

32 C. Liu and C. T. Martin, *J. Biol. Chem.*, 2002, **277**, 2725–2731.

33 H. Liu, J. Gao, S. R. Lynch, Y. D. Saito, L. Maynard and E. T. Kool, *Science*, 2003, **302**, 868–871.

34 H. Lu, K. He and E. T. Kool, *Angew. Chem., Int. Ed.*, 2004, **43**, 5834–5836.

35 E. L. Rachofsky, E. Seibert, J. T. Stivers, R. Osman and J. B. Ross, *Biochemistry*, 2001, **40**, 957–967.

36 P. K. Samanta, A. K. Manna and S. K. Pati, *Chem. – Asian J.*, 2012, **7**, 2718–2728.

37 P. K. Samanta, A. K. Manna and S. K. Pati, *J. Phys. Chem. B*, 2012, **116**, 7618–7626.

38 D. I. Scopes, J. R. Barrio and N. J. Leonard, *Science*, 1977, **195**, 296–298.

39 J. T. Stivers, *Nucleic Acids Res.*, 1998, **26**, 3837–3844.

40 R. A. Mizrahi, D. Shin, R. W. Sinkeldam, K. J. Phelps, A. Fin, D. J. Tantillo, Y. Tor and P. A. Beal, *Angew. Chem., Int. Ed.*, 2015, **54**, 8713–8716.

41 P. T. Ludford, 3rd, S. Yang, M. S. Bucardo and Y. Tor, *Chemistry*, 2022, **28**, e202104472.

42 M. Chawla, R. Credendino, R. Oliva and L. Cavallo, *J. Phys. Chem. B*, 2015, **119**, 12982–12989.

43 M. Chawla, R. Oliva, J. M. Bujnicki and L. Cavallo, *Nucleic Acids Res.*, 2015, **43**, 9573.

44 R. Oliva, L. Cavallo and A. Tramontano, *Nucleic Acids Res.*, 2006, **34**, 865–879.

45 R. Oliva, A. Tramontano and L. Cavallo, *RNA*, 2007, **13**, 1427–1436.

46 M. Chawla, R. Credendino, E. Chermak, R. Oliva and L. Cavallo, *J. Phys. Chem. B*, 2016, **120**, 2216–2224.

47 M. Chawla, S. Abdel-Azeim, R. Oliva and L. Cavallo, *Nucleic Acids Res.*, 2014, **42**, 714–726.

48 M. Chawla, R. Credendino, A. Poater, R. Oliva and L. Cavallo, *J. Am. Chem. Soc.*, 2015, **137**, 299–306.

49 H. N. Le, J. Kuchlyan, T. Baladi, B. Albinsson, A. Dahlen and L. M. Wilhelmsson, *Chemistry*, 2024, e202303539, DOI: 10.1002/chem.202303539.

50 A. F. Fuchtbauer, S. Preus, K. Borjesson, S. A. McPhee, D. M. J. Lilley and L. M. Wilhelmsson, *Sci. Rep.*, 2017, **7**, 2393.

51 A. F. Fuchtbauer, M. S. Wranne, S. Sarangamath, M. Bood, A. H. El-Sagheer, T. Brown, H. Graden, M. Grotli and L. M. Wilhelmsson, *ChemPlusChem*, 2020, **85**, 319–326.

52 A. Foller Larsen, B. Dumat, M. S. Wranne, C. P. Lawson, S. Preus, M. Bood, H. Graden, L. M. Wilhelmsson and M. Grotli, *Sci. Rep.*, 2015, **5**, 12653.

53 J. E. Sponer, K. Reblova, A. Mokdad, V. Sychrovsky, J. Leszczynski and J. Sponer, *J. Phys. Chem. B*, 2007, **111**, 9153–9164.

54 J. E. Sponer, N. Spackova, P. Kulhanek, J. Leszczynski and J. Sponer, *J. Phys. Chem. A*, 2005, **109**, 2292–2301.

55 J. E. Sponer, N. Spackova, J. Leszczynski and J. Sponer, *J. Phys. Chem. B*, 2005, **109**, 11399–11410.

56 P. Sharma, L. A. Lait and S. D. Wetmore, *PCCP*, 2013, **15**, 2435–2448.

57 A. D. Becke, *J. Chem. Phys.*, 1993, **98**, 5648–5652.

58 A. D. Becke, *Abstr. Pap., Jt. Conf. – Chem. Inst. can. Am. Chem. Soc.*, 1996, **212**, 112.

59 C. T. Lee, W. T. Yang and R. G. Parr, *Phys Rev B: Solid State*, 1988, **37**, 785–789.

60 T. H. Dunning, *J. Chem. Phys.*, 1989, **90**, 1007–1023.

61 A. Klamt and G. Schuurmann, *J. Chem. Soc., Perkin Trans. 2*, 1993, 799–805.

62 S. Grimme, J. Antony, S. Ehrlich and H. Krieg, *J. Chem. Phys.*, 2010, **132**, 154104.

63 C. Moller and M. S. Plesset, *Phys. Rev.*, 1934, **46**, 0618–0622.

64 F. Weigend and M. Haser, *Theor. Chem. Acc.*, 1997, **97**, 331–340.

65 S. F. Boys and F. Bernardi, *Mol. Phys.*, 1970, **19**, 553.

66 P. Sharma, S. Sharma, M. Chawla and A. Mitra, *J. Mol. Model.*, 2009, **15**, 633–649.

67 M. Chawla, P. Sharma, S. Halder, D. Bhattacharyya and A. Mitra, *J. Phys. Chem. B*, 2011, **115**, 1469–1484.

68 C. L. Zirbel, J. E. Sponer, J. Sponer, J. Stombaugh and N. B. Leontis, *Nucleic Acids Res.*, 2009, **37**, 4898–4918.

69 A. Mladek, P. Sharma, A. Mitra, D. Bhattacharyya, J. Sponer and J. E. Sponer, *J. Phys. Chem. B*, 2009, **113**, 1743–1755.

70 M. Chawla, Y. Minenkov, K. B. Vu, R. Oliva and L. Cavallo, *ChemBioChem*, 2019, **20**, 2262–2270.

71 M. Chawla, I. Autiero, R. Oliva and L. Cavallo, *Phys. Chem. Chem. Phys.*, 2018, **20**, 3699–3709.

72 R. Bauernschmitt and R. Ahlrichs, *Chem. Phys. Lett.*, 1996, **256**, 454–464.

73 M. E. Casida, C. Jamorski, K. C. Casida and D. R. Salahub, *J. Chem. Phys.*, 1998, **108**, 4439–4449.

This journal is © the Owner Societies 2024

Phys. Chem. Chem. Phys., 2024, **26**, 16358–16368 | **16367**

74 R. E. Stratmann, G. E. Scuseria and M. J. Frisch, *J. Chem. Phys.*, 1998, **109**, 8218–8224.

75 M. Chawla, A. Poater, P. Besalu-Sala, K. Kalra, R. Oliva and L. Cavallo, *Phys. Chem. Chem. Phys.*, 2018, **20**, 7676–7685.

76 M. Chawla, A. Poater, R. Oliva and L. Cavallo, *Phys. Chem. Chem. Phys.*, 2016, **18**, 18045–18053.

77 P. V. Schleyer, C. Maerker, A. Dransfeld, H. J. Jiao and N. J. R. V. Hommes, *J. Am. Chem. Soc.*, 1996, **118**, 6317–6318.

78 K. Wolinski, J. F. Hinton and P. Pulay, *J. Am. Chem. Soc.*, 1990, **112**, 8251–8260.

79 J. Poater, M. Duran, M. Sola and B. Silvi, *Chem. Rev.*, 2005, **105**, 3911–3947.

80 N. B. Leontis, J. Stombaugh and E. Westhof, *Nucleic Acids Res.*, 2002, **30**, 3497–3531.

81 N. B. Leontis and E. Westhof, *RNA*, 2001, **7**, 499–512.

82 M. J. Cavaluzzi and P. N. Borer, *Nucleic Acids Res.*, 2004, **32**, e13.

83 D. Onidas, D. Markovitsi, S. Marguet, A. Sharonov and T. Gustavsson, *J. Phys. Chem. B*, 2002, **106**, 11367–11374.

84 E. R. Johnson, S. Keinan, P. Mori-Sanchez, J. Contreras-Garcia, A. J. Cohen and W. Yang, *J. Am. Chem. Soc.*, 2010, **132**, 6498–6506.

85 R. A. Boto, F. Peccati, R. Laplaza, C. Quan, A. Carbone, J. P. Piquemal, Y. Maday and A. J. Contreras-Garci, *J. Chem. Theory Comput.*, 2020, **16**, 4150–4158.

16368 | *Phys. Chem. Chem. Phys.*, 2024, **26**, 16358–16368

This journal is © the Owner Societies 2024